2015

Analysis of steady state micro-droplet evaporation to enhance heat dissipation from tiny surfaces.

Harish Voota
University of Central Florida

ANALYSIS OF STEADY STATE MICRO-DROPLET EVAPORATION TO ENHANCE HEAT DISSIPATION FROM TINY SURFACES

by

HARISH VOOTA
M.S. University of Central Florida, 2015

A thesis submitted in partial fulfillment of the requirements
for the degree of Master of Science
in the Department of Mechanical and Aerospace Engineering
in the College of Engineering and Computer Science
at the University of Central Florida
Orlando, Florida

Summer Term
2015

Major Professor: Shawn A. Putnam

ABSTRACT

Experimental investigations and numerical predictions of steady state microdroplet evaporation experiments are presented. Steady state droplet evaporation experiments are conducted to understand (1) Droplet contact line influence on evaporation rate efficiency, (2) Droplet contact angle correlation to evaporation rate and (3) Substrate cooling. Experiments are performed on a polymer substrate with a moat like trench (laser patterned) to control droplet contact line dynamics. A bottom-up methodology is implemented for droplet formation on the patterned substrate. Droplet evaporation rates on substrate temperatures 22℃$\leq \Delta T_{Substrate} \leq$75℃ and contact angles 80°$\leq \Theta \leq$110° are measured. For a pinned microdroplet (CCR), volumetric infuse rate influences droplet contact angle. Results illustrate droplet contact line impact on evaporation rate. Moreover, these results coincide with previously published results and affirm that evaporation rate efficiency reduces with contact line depinning. Additionally, from all the analyzed experimental cases, evaporation rate scales proportional to the microdroplet contact angle (i.e. $\dot{m}_{LG} \propto \theta$). In conclusion, these experiments shed new light on steady state evaporation of a microdroplet and its corresponding observations. Vital research findings can be used to enhance heat dissipation from tiny surfaces.

ACKNOWLEDGMENTS

I would like to express the deepest appreciation to my advisor Dr. Shawn Putnam, who gave me an opportunity to work in his group and thus on the project. He continually and persuasively conveyed a spirit of encouragement in regard to research and scholarship. Without his supervision and constant help this thesis would not have been possible. I would also like to thank my thesis committee members, Dr. Jeffrey Kauffman and Dr. Subith Vasu, for their time. I still remember being in the first month of my master‘s when Dr. Kauffman referred me to Dr. Shawn Putnam (my advisor) for a graduate research assistant position. This position not only gave me a part time job but also an opportunity to explore my potential. I am more than contended to have started my masters with his advice and ended it with his approval on the thesis committee form. In addition, I acknowledge Dr. Subith Vasu‘s guidance and support during my master‘s.

My sincere thanks to lab mate, Kevin Gleason for his continuous support during research and experiments. I bow to his immense subject knowledge and ever helping nature. He has shown the attitude and substance of a genius. I wish him success for his journey at Yale University for a PHD. I also want to thank my other fellow lab mate, Mehrdad Mehrvand for wise advises and fun conversations over the years. Additionally, I acknowledge my friend and fellow graduate researcher at UCF, Kalpana Madhushan for helping me out with all the tuff courses during master‘s. I am in debt to the help he offered me.

This project would not have been possible without the financial support of Mechanical and Aerospace Engineering‘s graduate teaching assistantship cum scholarship program. It saved me lot of money and gave me a peace of mind to work passionately. A heartfelt thanks to University of Central Florida for the opportunity, it has built me to Reach for the Stars.

Last but not the least, I would like to mention my family: Mallikarjuna Rao Voota, Madhavi Voota, Harika Voota and Bhanu Thota for helping, loving and supporting me all my life. Thank you!

TABLE OF CONTENTS

LIST OF FIGURES

NOMENCLATURE

A	Area
h	Apex Height
$\dot{m}_{\text{evap}}$	Evaporation Rate
$\dot{m}_{\text{pump}}$	Syringe Pump Infuse Rate
R	Contact Radius
T_0	Setpoint Temperature
T_s	Substrate Temperature
t	Thickness
V	Volume
W	Watts

Greek

γ	Surface Tension
Δ	Difference/Change in
κ	Thermal Conductivity
θ	Contact Angle

Acronyms

CCA	Constant Contact Angle
CCR	Constant Contact Radius
DI	Deionized
IR	Infrared

CHAPTER 1: INTRODUCTION

A fundamental process like droplet evaporation which is widely observed in day to day life holds a pivotal role in many technical applications like DNA/RNA micro-array deposition [1, 2], inkjet printing [3, 4], cooling electronic devices [5–7], combustion [8, 9] and metrology [10, 11]. Rate of evaporation holds key for these application‘s efficiency. A droplet evaporation rate is influenced by contact line dynamics[7, 12–14], substrate conductivity [15], vapor concentration [16] and intermolecular forces [17, 18].

Contact line dynamics of a droplet is directly associated with influencing evaporation rate. Recently, Zhang et al. [19] explained the role played by surface tensions due to the curvature of solid-liquid-vapor contact line as a correction to Young‘s equation. Also, Putnam et al. [7] reported evaporation rate decrease with contact line de-pinning. Droplet evaporation experiments on a heated substrate reported a temperature gradient between solid-liquid/liquid-gas interfaces proportional to substrate thermal conductivity [15]. Moreover, highly conductive surfaces explain contact line region to be hotter than rest of the droplet causing thermo-capillary convection within the bulk of the droplet and a re-circulation flow to occur from droplet contact line to droplet center [20, 21].

Convection in gas domain is an important transport mechanism governing droplet evaporation. Vapor concentration gradient between droplet surface (i.e., liquid-vapor interface) and its surrounding air induces natural convection in gas phase [16, 22, 23]. Consequently, gas phase convection influence vapor transport and thus evaporation rate [24]. For example, the evaporative heat flux scales inversely with relative humidity [25]. Furthermore, heat transfer characteristic is sensitive to chemical bonding [17, 18]. For a droplet evaporation process, inter-molecular forces in liquid-vapor phase creates an activation energy barrier for

a liquid phase molecule to join vapor phase [26]. In addition, surfactants are also reported to have influence on droplet evaporation. Recently, nanoparticles in fluid have been a great research interest due to their effect on wetting behavior of the fluids. Nanoparticles tend to pin the contact line and are calculated to be in proportion to de-pinning energy barrier [27–30].

In 1977, Picknett and Bexon [31] introduced two extreme modes of droplet evaporation, namely constant contact radius mode (CCR) and constant contact angle mode (CCA). Droplet contact radius remains fixed (pinned) with gradual decrease in contact angle during constant contact radius mode (CCR) whereas in constant contact angle mode (CCA) droplet contact angle tends to remain constant with receding contact radius. Today, A dynamic droplet evaporation process is classified under four modes: constant contact radius mode (CCR), constant contact angle mode (CCA), mixed mode [32] (gradual decrease in both contact angle and contact radius) and stick-slip mode [33] (rapid pinning and de-pinning of contact line). Nguyen et.al [34] reported a non-linear evaporation rate for a dynamic evaporation process due to different evaporation modes. Since last two decades much has been studied, investigated and understood about the droplet evaporation process, please check references [7–15, 17, 32, 33, 35–47].

Several vapor diffusion based models have been used to predict interfacial evaporation flux and overall evaporation rate [34, 48–51]. Hu & Lardon [20] used finite element method to investigate vapor diffusion during droplet evaporation. Popov [52] used Deegan‘s model [53] to predict evaporation rates at different contact angles. Popov‘s model predicted: firstly, for wetting contact angles ($\Theta < 90°$) evaporation flux diverges at contact line, secondly for non-wetting contact angles ($\Theta > 90°$) flux is highest at apex of the droplet than any other part of the droplet and finally, at contact angle ($\Theta = 90°$) flux is constant along the interfacial contact line. However, a constant vapor concentration model at droplet interface overlooks principles like evaporative cooling and droplet thermal resistance during the evaporation process. Thus,

Popov‘s model validation at greater contact angles and highly conductive substrates is being discussed. Experimentally it was reported that a liquid to vapor phase change causes droplet liquid-vapor interface to cool due to latent heat of absorption [54]. Also, recently Stauber et.al [55] reported evaporative cooling to increase with instantaneous contact angle of the droplet. Therefore, Gleason and Putnam [46] improvised upon Popov‘s model by including temperature distribution along the liquid-vapor interface. Total evaporation flux predictions by Popov‘s model and its modified/improvised model by Gleason and Putnam are compared with experimental results in section (4.2 and 4.3).

The specific problem of understanding evaporation rate correlation to droplet extreme modes (i.e., CCR & CCA) still persist. Experimentally, a series of approximations have been used in past to understand these correlations. Focus of this work is to (1) develop a controlled droplet evaporation mode with both the constant contact radius and constant contact angle (CCR & CCA) and (2) understand evaporation rate correlation to droplet evaporation modes.

CHAPTER 2: EXPERIMENTAL DETAILS

2.1. Materials

A clear acrylic polymer disk (1 inch diameter & 0.25 inch thickness) is used as a substrate. The substrate surface is micro patterned to make a circular shaped trench. This circular shaped trench keeps radius fixed or pinned. Fabricating a pattern spot on the polymer substrate of depth $\delta \approx 50\mu$m and radius R $\approx 450\mu$m can be referenced [56]. Deionized water is used for all the experiments. It is passed through a 0.2μm filter prior to use.

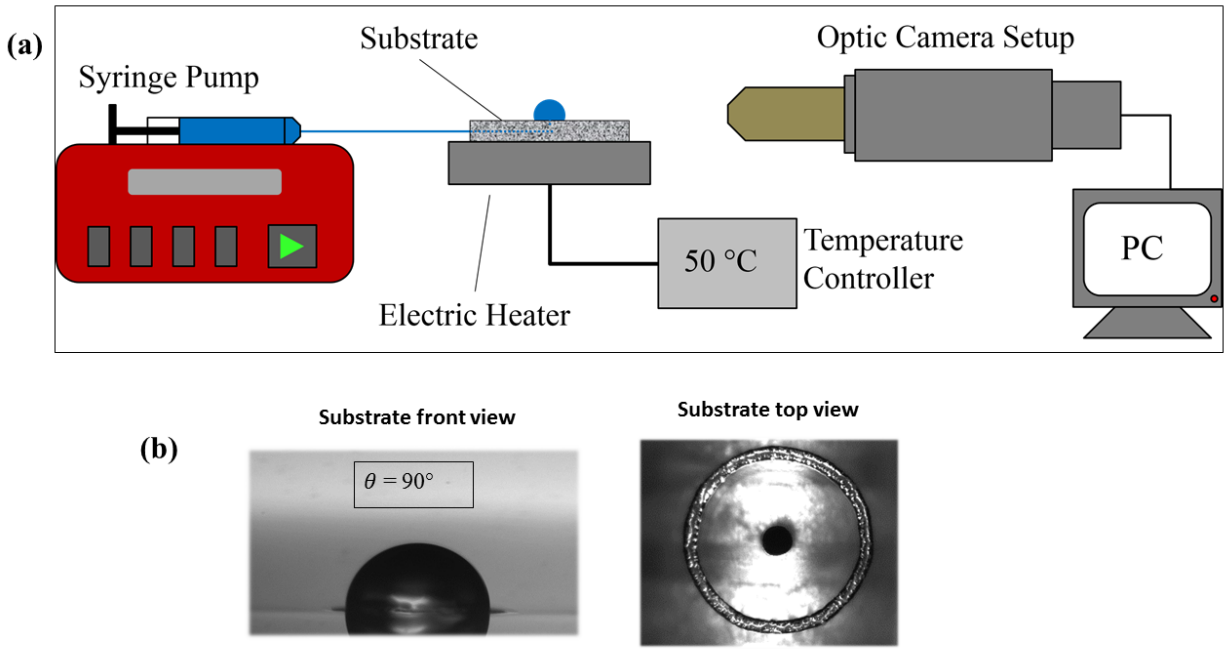

Figure 2.1: (a)Schematic of experimental setup for a controlled microdroplet evaporation experiment. (b) Patterned substrate profile.

2.2. Steady-State Microdroplet Evaporation Measurements

Figure 2.1 shows schematic of the experimental setup for steady state microdroplet evaporation. Computer controlled syringe pump drives water through a micro-channel implementing bottom-up methodology, connecting syringe exit to cavity at center to laser patterned circular trench. A Temperature controller coupled with $\sim 75\Omega$ electric heater is used to regulate substrate temperature ($T_{Substrate}$) within ± 1.5℃. A computer controlled CCD camera coupled with microscopic objective optics and LabView software is used for video recording. A customized LabView program is used for image analysis [7, 10]. The greyscale edge detection technique through image analysis software measures micro droplets apex height (H), contact radius (R) and contact angle (Θ) by fitting a circle to best edge/ contour of the microdroplet. Volume (V) is calculated by spherical cap volume equation [7].

Relative humidity with an error measurement of $\pm 2\%$ was monitored and measured during all the experiments. To avoid air bubble nucleation/formation the water was degassed in by vacuum pump. Steady state droplet formation requires two different volume flow rates, first flow rate to form a droplet with stable initial volume for a certain contact angle and second flow rate to balance the evaporation rate of a microdroplet. For example, building a steady state droplet with contact angle $\approx 110^{\circ}$at 60℃and 45% relative humidity requires a first volumetric flow rate of 10nL/sec to form a $\approx$ 380nL droplet, then the flow rate is decreased to $\sim$5 nL/sec for steady state evaporation. Evaporation rate was experimentally verified by stopping the syringe pump after several minutes of steady state droplet evaporation and then analyzing the rate of decrease of droplet volume. To avoid error in measurement, evaporation rate is only calculated until 97% of depinned contact radius R_0.

CHAPTER 3: NUMERICAL SIMULATIONS

The rate of droplet evaporation on a heated substrate is dictated by the concentration gradient between the droplets liquid-vapor interface and ambient environment. A diffusion-limited model is evaluated to compare the experimentally measured infuse/evaporation rates, shown in Equation (1). The experimentally measured contact radius (R) and contact angle (Θ) during steady-state evaporation are used to perform a single evaluation of the evaporation rate ($\frac{dm}{dt}$). The diffusion coefficient (D) and ambient concentration (c_∞) are calculated using the temperature and relative humidity measured during each experiment to accurately represent the data.

$$\dot{m}_{lv} = -\pi RD(c_s(\alpha,\theta) - c_\infty)\left[\frac{\sin\theta}{1+\cos\theta} + 4\int_0^\infty \frac{1+\cosh 2\theta\tau}{\sinh \pi\tau}\tanh\left[(\pi-\theta)\tau\right]d\tau\right]. \quad (3.1)$$

This model is a modified version of the diffusion-limited model reported by Popov [4] which integrates a solution of the local evaporation flux along the entire liquid-vapor interface. The model, which initially considers the concentration along the liquid-vapor interface (c_S) a constant, has shown to deviate from experimental measurements when evaporative cooling and convection effects are present [24, 44, 56–58]. High fidelity models capturing this neglected phenomenon have shown to accurately predict evaporation rates for most practical contact angles ($10^\circ \leq \Theta \leq 170^\circ$) [24].

The modification in the presented model accounts for the evaporative cooling effect by introducing a temperature dependent surface concentration along the liquid vapor interface, $c_S(\alpha, \Theta)$. This distribution is estimated using a mapping function, correlating the temperature and saturation concentration to a location along the droplets liquid-vapor interface (α)

for a given droplet contact angle (Θ) [56]. This a simpler approach compared to sophisticated simulations, and have shown to provide sufficient predictions for sub millimeter water droplets as presented in this study.

CHAPTER 4: EXPERIMENTAL RESULTS

4.1. Steady state micro-droplet evaporation

A microdroplet evaporating with constant droplet parameters over a time period is considered to be at steady state. Droplet parameters: volume (V), radius (R), contact angle (Θ) and height (H) are considered. Technically, volumetric equilibrium of infuse and evaporation flow rates result into a steady state droplet. The volume of water entering a spherical droplet through bottom-up methodology equals volume evaporating through droplet's spherical surface. A laser patterned acrylic substrate pins the droplet contact line. Radius of the laser patterned substrate is $R_{Substrate} \cong 450\mu$m. Droplet contact line pinning leads to droplet contact angle variation. Furthermore, infuse fluid flow rate variation determine changes to droplet contact angle.

Fig. 4.1(a) represents a steady state droplet evaporating on a heated surface. Changes in droplet parameters are captured and recorded by an imaging system (high speed camera with 20X objective).Droplet evaporation profile is calculated by LabView software using a customized image analysis code. Droplet volume, contact angle, contact radius, volume infuse rate and evaporation rate are measured. The set point droplet parameters radius (R_0) and contact angle (Θ_0) are basic reference parameters for running the experiment and calculating the error in measurements. Figure 4.1(b) represents a graphical illustration of an evaporating droplet at substrate temperature $T_{Substrate} \approx 40$℃and relative humidity 50%. Volume of the evaporating droplet is $\cong$ 224 nL for more than five minutes, depicting a volumetric evaporation rate to infuse rate balance. Vertical dotted lines in the figure represent the period with constant droplet parameters. All parameters for experimental and numerical analysis are calculated during this period.

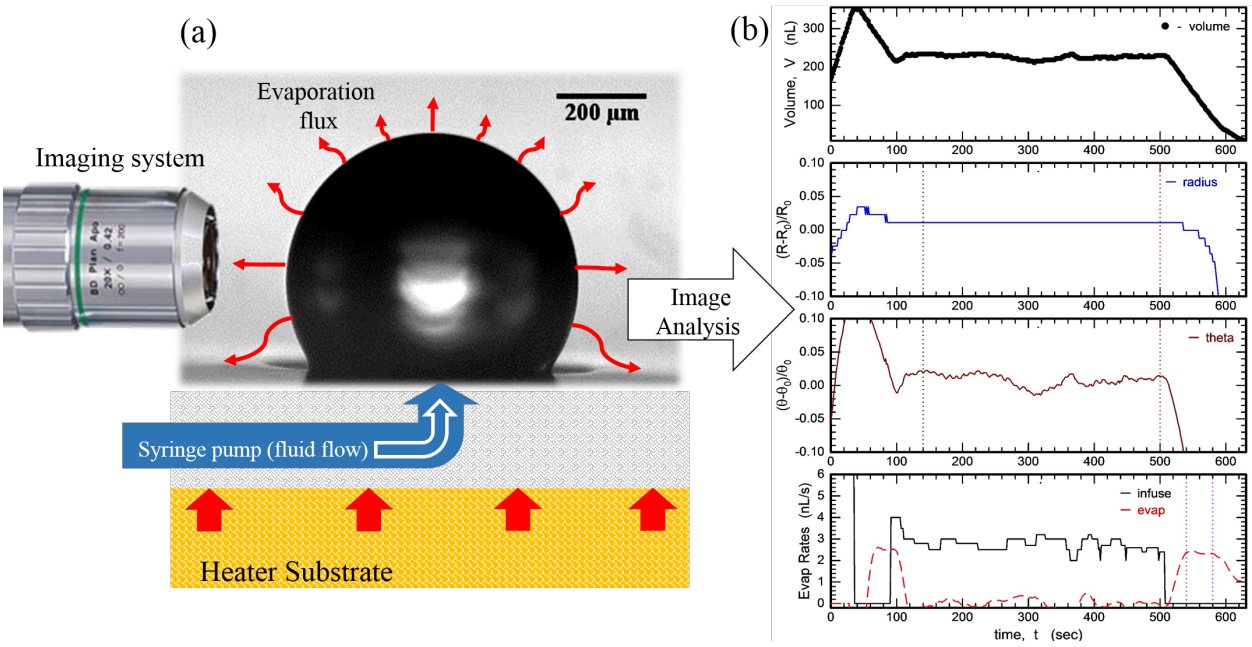

Figure 4.1: (a) Schematic diagram of the steady state microdroplet evaporation experiment. (b) Plots of Droplet parameters as a function of time (t). Vertical dotted lines represent steady state evaporation period. Experimental Details: $T_{Substrate} \cong 40$℃, R.H = 50%, Volume(V) = 224 ± 5nL, Contact radius(R) = 454μm ± 0.1μm, Setpoint radius(R_0) = 450μm, Contact angle(Θ) = 95.3°± 0.8, Setpoint angle(Θ_0) = 95°, Volume infuse flow rate = 2.75 ± 0.3 nL/s and Volume evaporation rate = 2.33 ± 0.3 nL/s.

Contact angles of a microdroplet are explained by Young-Laplace equation. For curved surfaces, surface tension causes a pressure difference between the interfaces,dP. Pressure difference is directly proportional to cosecant of contact angle, since contact radius is pinned (constant) for steady state microdroplet evaporation process. The change in Laplace pressure for these volume fluctuations is small (e.g., ΔP ∼0.01 kPa for $\Delta\Theta$ ∼ 2°deg). Pressure variance, dP in the micro channel connecting syringe to the substrate can be neglected in comparison to dP at droplet curved surface interface. At contact angles $\Theta > 90$°an outward force on the droplet interface naturally holds a stable droplet for a longer time period, whereas at contact angles $\Theta < 90$°an impeding force on the droplet interface causes an unstable droplet if infuse rate and evaporation rate are not in equilibrium. Steady state evaporation experiments are conducted with droplet contact angles $\Theta \in$(80°,95°& 110°) on temperatures 22℃≤ $\Delta T_{Substrate}$ ≤80℃. Each experiment with a specific substrate temperature and contact

angle is repeated to reproduce results. Best of five measurements are used to reduce error in measurement. These experiments are conducted to understand evaporation rate relationship with droplet contact angle and contact radius.

4.2. Droplet influence on substrate temperature

Results are presented in this section to understand the influence of water droplet evaporation on a heated substrate. A water droplet with constant contact angle ($\sim$110°) and pinned contact radius ($\sim$450μm, due to pattered substrate) is used. These experiments are conducted on set point temperatures 30℃$\leq \Delta T_0 \leq$80℃. Set point temperatures are manually controlled with electric heater/temperature controller. A manually controlled set point temperature varies from temperature recorded on the substrate surface. An Infrared camera is used to record and analyze substrate temperatures.

Figure 4.2(a) presents infrared images of 0.25 inch thick heated substrate. These images compare substrate temperature distribution with and without water droplet. Substrate temperatures at the patterned trench with/without water droplet are compared. Lowest substrate temperature used is $T_{Substrate} \cong$ 31℃. A pinned water droplet produces changes in substrate temperature distribution and generates substrate cooling. Temperature of the substrate near the patterned trench reduces to $\cong$ 30℃. Similar experiments are done on higher temperatures to understand the temperature difference and substrate cooling effect. Highest substrate temperature used is $T_{Substrate} \cong$ 68℃. At this temperature, a pinned droplet reduce the substrate temperature by $\cong$ 4℃. Infrared camera records the substrate temperature as $T_{Substrate} \cong$ 64℃at the patterned trench. Figure 4.2(b) compares substrate cooled temperatures ($T_{Substrate\ cooled}$) to substrate temperatures ($T_{Substrate}$). Substrate cooled temperatures represent substrate temperatures with a water droplet. Temperature difference ($T_{Substrate}$ - $T_{Substrate\ cooled}$) varies between $\cong$ 1℃to $\cong$ 4℃from lowest to the highest temperature.

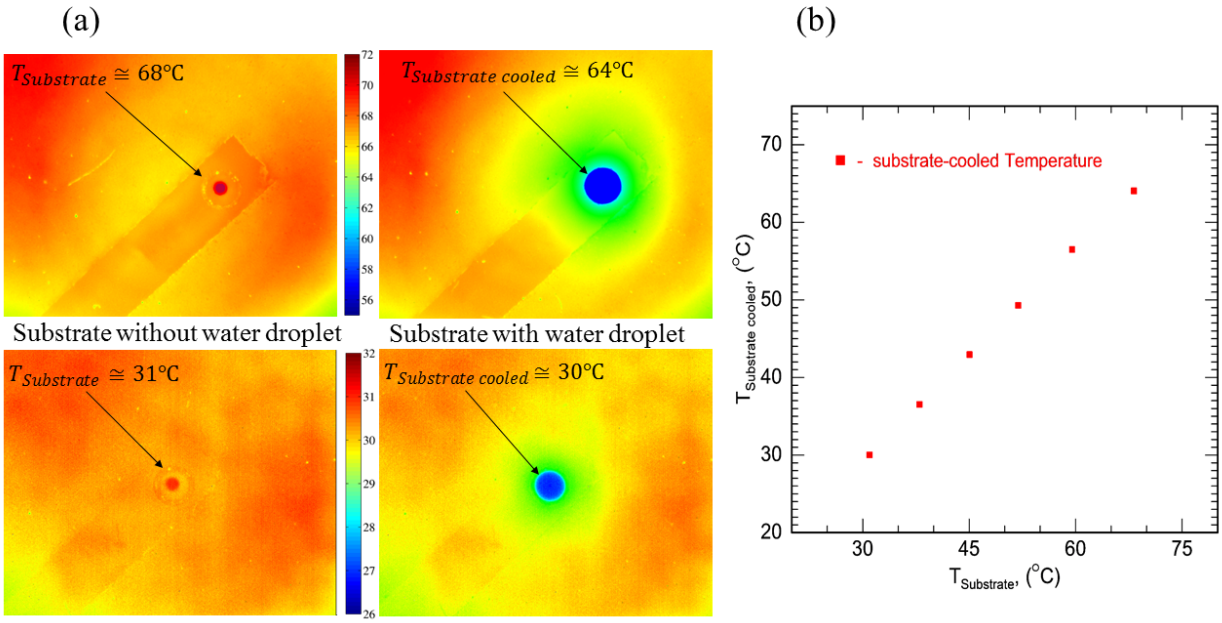

Figure 4.2: (a) Infrared camera recorded substrate images. Image details: $T_{Substrate}$ (without water droplet) ≅ 68℃, $T_{Substrate\ cooled}$ (with water droplet) ≅ 64℃.$T_{Substrate}$ (without water droplet) ≅ 31℃, $T_{Substrate\ cooled}$ (with water droplet) ≅ 30℃. (b)Temperature of substrate with droplet cooling is compared to temperature of substrate without droplet. Experiments are performed on temperature range 30℃≤ $T_{Substrate}$ ≤70℃.

Figure 4.3 (a) represents temperature distribution of a heated substrate influenced by a pinned water droplet. An infrared camera's image oriented temperature scale illustrates temperature distribution over the substrate. The image represents substrate at set point temperature T_0 ≅ 60℃. Since set point temperature and infrared camera analyzed temperature vary, substrate temperature at ∼ 800μm and ∼ 2500μm from the center are compared. A relatively cool water droplet on a heated substrate tends to absorb heat and produce substrate cooling. Temperature of substrate increases along the direction away from the droplet. Similar experiment is performed on set point temperatures 30℃≤ ΔT_0 ≤80℃. Figure 4.3 (b) shows infrared camera analyzed temperatures compared to set point temperatures. Furthermore, infrared camera analyzed temperatures at different substrate locations ∼ 800μm ($T_{Substrate\ cooled}$) and ∼ 2500μm ($T_{Substrate}$) are compared. Temperature distri-

bution at different surface locations explain the droplet cooling effect. At lower set point temperatures, temperature distribution over the substrate surface tends to remain nearly constant $T_{Substrate\ cooled} \cong T_{Substrate}$. Droplet cooling has a lesser impact on substrate surface at lower set point temperatures. Whereas, increase in set point temperatures increase droplet cooling impact. As illustrated in figure 4.3 (b), temperatures at 800 μm and 2500 μm from the center differ by $\sim$4℃at highest set point temperature $T_0 \cong$ 80℃.

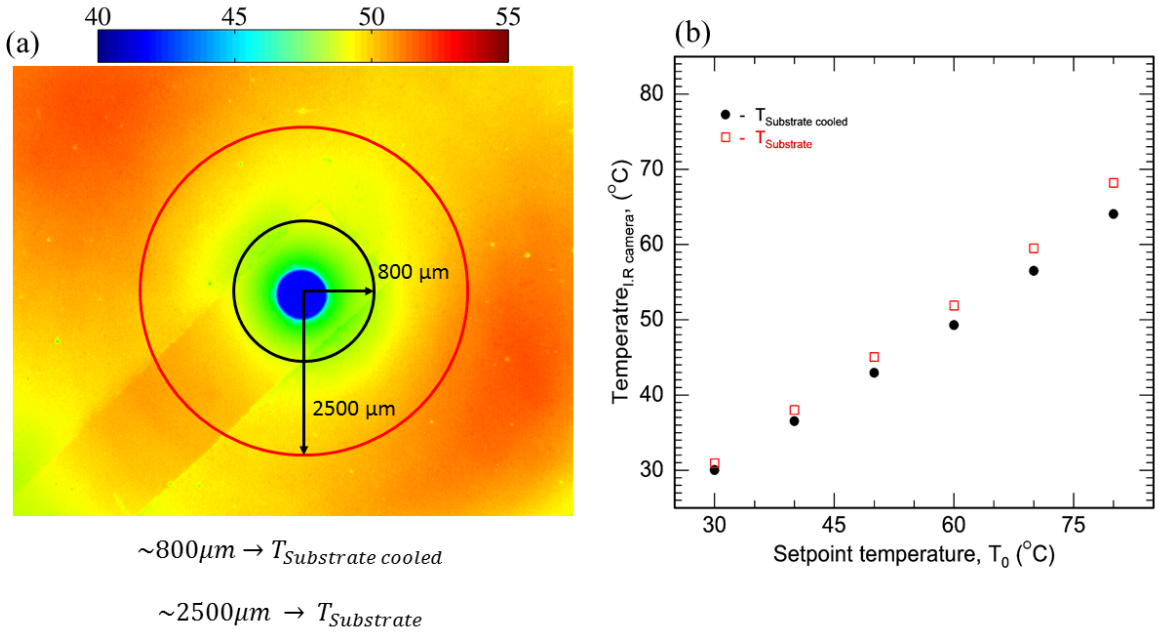

Figure 4.3: (a) Temperature controller controlled set point temperatures are compared to infrared camera temperature readings of a polymer acrylic substrate. $T_{Substrate\ cooled}$ refers to temperature near to laser patterned trench influenced by substrate cooling due to droplet formation. $T_{Substrate}$ refers to substrate temperature near to substrate edge. (b) Experimental data: $T_{Substrate\ cooled}$ (black dot), $\sim$ 800μm from center of substrate. $T_{Substrate}$ (red square), $\sim$ 2500μm from center of substrate. Experiments performed on set point temperatures 30℃ $\leq T_0 \leq$ 80℃.

4.3. Droplet contact line influence on evaporation efficiency.

Droplet contact line influence on evaporation efficiency has been long discussed [13, 15, 38, 59]. It is a vital parameter influencing heat flux off droplet liquid-vapor interface. Results of droplet evaporation experiments in the past have correlated contact line dynamics to evaporation rates. It has been understood that evaporation rate decreases with contact line depinning [7, 13]. Evaporation efficiency for droplet evaporation process can be explained as a comparison of volumetric infuse flow rate into a droplet to volumetric evaporation flow rate off the droplet surface.

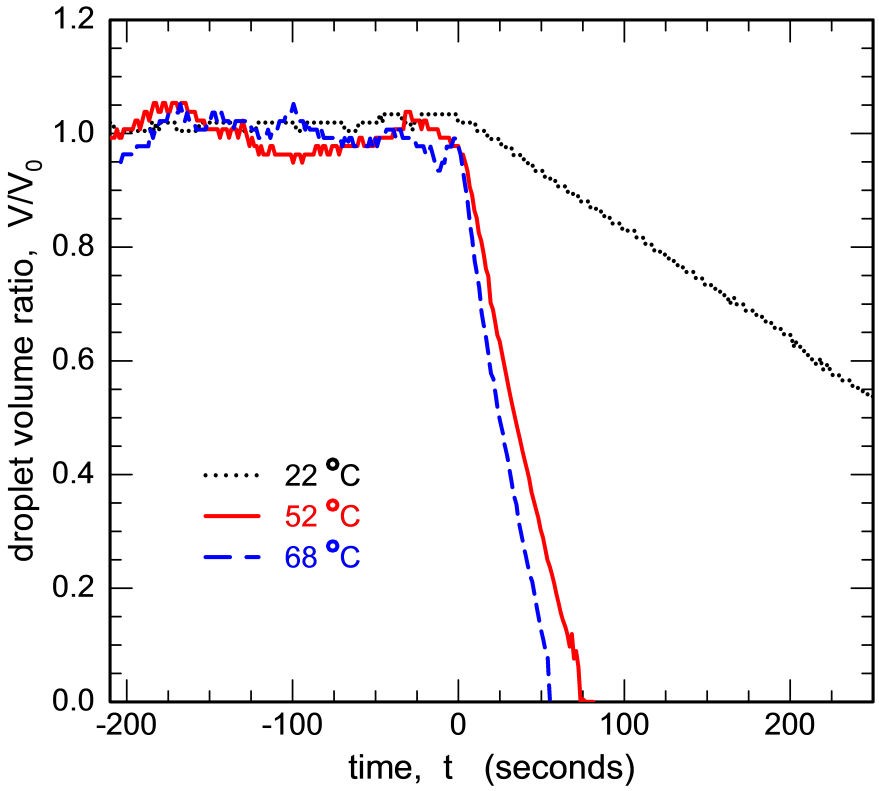

Figure 4.4: Dimensionless droplet volume (V/V_0) as a function of time for water microdroplet evaporation on heated and unheated polymer substrates. $T_{I.R} \cong$ 22℃, 51.90℃and 68.20℃are infrared camera temperature readings of the substrate for controlled setpoint temperatures $T_0 =$ 22℃,60℃and 80℃respectively. V_0 is droplet volume at the onset of steady-state evaporation and time,(t=0 seconds) represents fluid pump stopped. Experimental Details: $T_{I.R} \cong$ 22℃- {RH = 54%, $V_0 \cong$ 346 nL, $\Theta_0 \cong 110^{\circ}$, $R_0 \cong$ 452 μm}; $T_{I.R} \cong$ 51.90℃ {RH = 45%, $V_0 \cong$ 345 nL, $\Theta_0 \cong 110^{\circ}$, $R_0 \cong$ 450 μm}; $T_{I.R} \cong$ 68.20℃- {RH = 51%, $V_0 \cong$ 350 nL, $\Theta_0 \cong 110^{\circ}$, $R_0 \cong$ 452 μm}.

Figure 4.4 presents non-dimensionalized droplet volume at set point temperatures (T_0 $\approx$ 22℃, 60℃and 80℃) plotted over time. Infrared camera measured substrate temperatures for the respective set point temperatures are $T_{Substrate} \approx$ 22℃,52℃and 68℃. Plot illustrates droplet evaporation process from steady state evaporation phase (with constant infuse flow rate) to unsteady evaporation phase (without infuse flow rate). Steady state evaporation phase is represented by time in negative and unsteady phase by time in positive. Time, t=0 seconds on the plot shows fluid injection pump being stopped and the beginning of unsteady evaporation phase. All experiments are conducted at contact angle $\Theta \cong 110$˚on laser patterned substrate to keep contact radius pinned. Evaporation period at this contact angle gives enough data points to increase data efficiency. Evaporation rate is known during steady state evaporation period since manually controlled infuse flow rate equals evaporation rate during the period. For unsteady evaporation phase, evaporation rate is calculated from the recorded data from the time syringe pump is stopped until contact radius depinning. Infuse to evaporation flow rate measurements in figure 4.5 are explained though this figure.

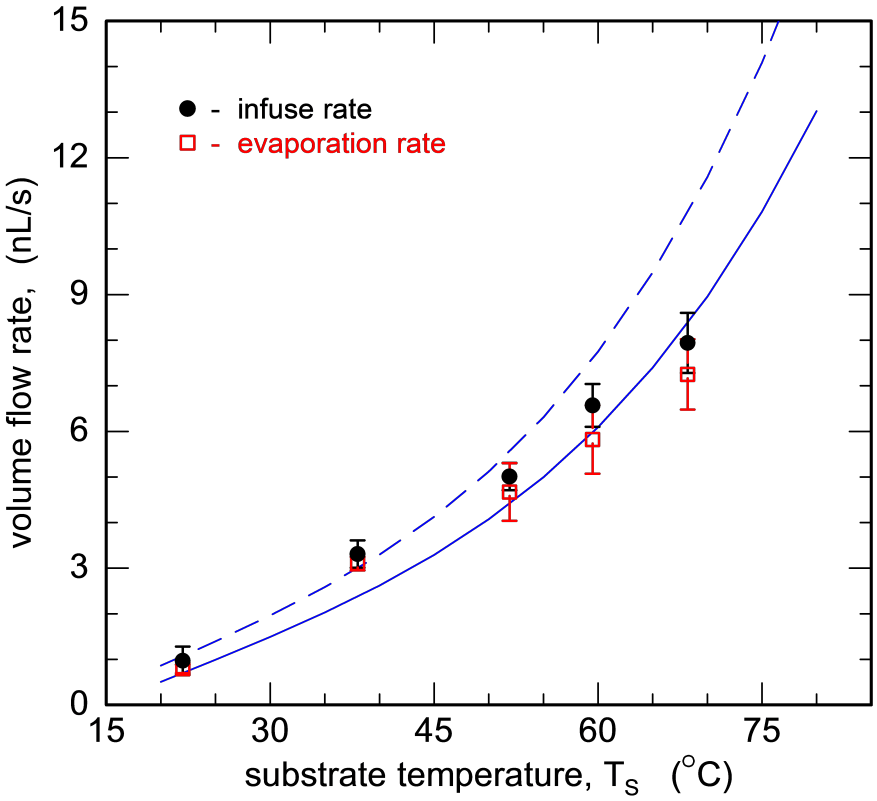

Figure 4.5: Comparison between the water infuse rate (i.e., steady-state evaporation rate at constant contact angle) and the unsteady evaporation rate for water micro-droplet evaporating at different substrate temperatures $T_{Substrate} \cong$ 22℃, 38℃, 52℃, 59.5℃and 68.20℃. The unsteady evaporation rate is calculated for $0.97R_0 \leq \mathrm{R} \leq R_0$. Plot also compares numerical simulation results obtained from Popov's model (Dashed line) and modified Popovs model with variable surface concentration (solid line). Experimental Details: { $\Theta_0 = 110 \pm 1^{\circ}$, $V_0 = 340 \pm 10.3$ nL, $R_0 = 450 \pm 4.7$ μm }.

Figure 4.5 presents infuse to evaporation flow rate measurements plotted over substrate temperatures 22℃ $\leq T_{Substrate} \leq$ 70℃. Figure explains evaporation efficiency for pinned droplet and describes the effect of depinning on microdroplet evaporation rate. Individual steady state evaporation experiments are conducted at different substrate temperatures to measure infuse and evaporation flow rates. A best of five experiments are used to reduce measurement error and generate error bars. At a substrate temperature, Infuse flow rate into a steady state evaporating droplet is compared to evaporation flow rate of droplet with fluid pump switched off. The measured evaporation rate is dynamic since droplet evaporation is not controlled. It is measured till 97% of depinned contact radius. Results show that

infuse rate equals measured evaporation rate until the contact radius depins to a value less than $0.97R_0$. Volume flow rate predictions by Popov's model [52] and modified Popovs model [56] are compared to experimental results. Modified model tends to coincide with the experimental results for substrate temperatures $T_{Substrate} \geq 50$℃. Experimental results at lower temperatures agree more to Popov's model. A good agreement is achieved as expected, evaporation rate reduces with contact line depinning. Moreover it explains that evaporation efficiency remains constant for pinned contact radius.

4.4. Droplet contact angle influence on evaporation rate.

Literature review points out that hydrophobic and hydrophilic surfaces have been used to understand a droplet contact angle to evaporation rate correlation. On a heated substrate, microdroplet with contact angle $\Theta > 90$°is observed to be more stable than microdroplet with contact angles $\Theta < 90°$. Interestingly, liquid-vapor contact line has a significant influence on the heat transfer performance. Additionally, Droplet heating on a substrate also noted a fast and rapid decrease in contact angle below $\Theta < 70°$[47]. However, theoretical predictions and experimental results have shown that evaporation time for sessile droplet with acute contact angle is shorter than droplet with obtuse angle having same volume [60, 61]. It has also been concluded that at constant volumes, rate of evaporation is faster for smaller droplets [18, 20, 31, 62]. These experiments were not conducted at constant contact radius mode (CCR). Thus a firm correlation between contact angle and evaporation rate was not made. Evaporation rate is a function of droplet volume and at constant contact radius mode (CCR), evaporation rate tends to depend upon contact angle [43–46].

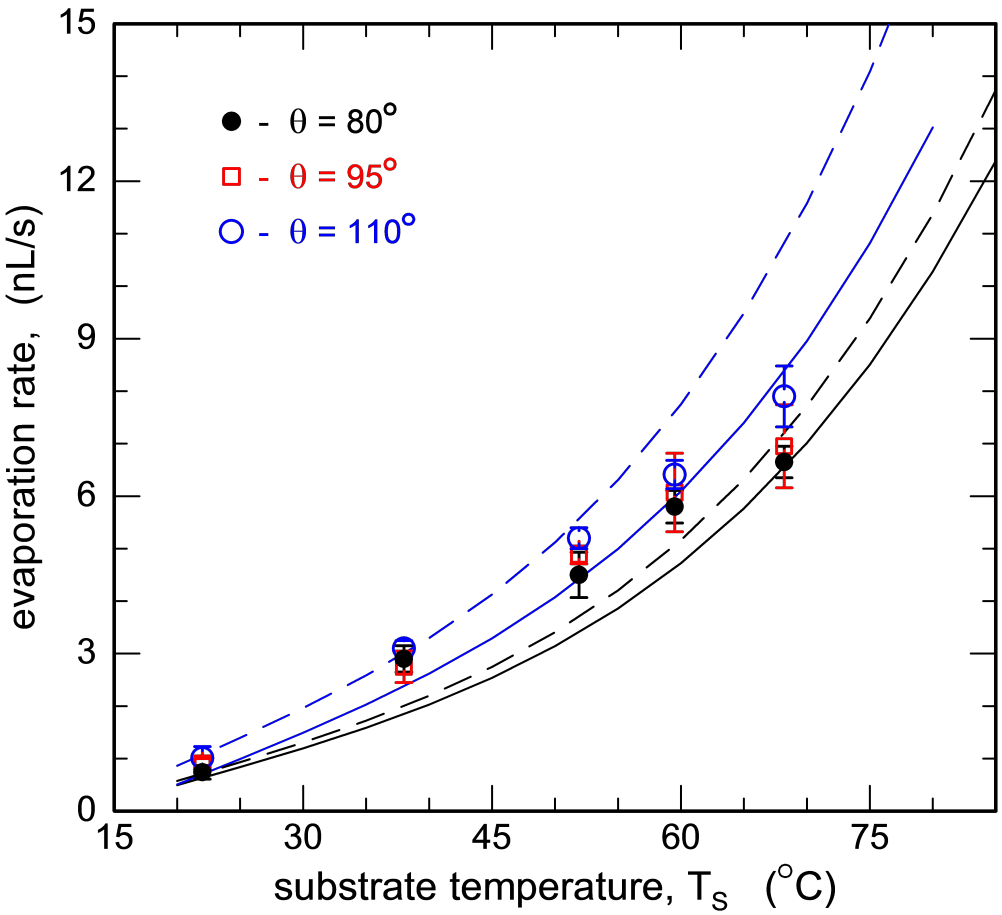

Figure 4.6: Popov's model predictions (dashed lines), modified popov's model predictions (solid lines) and measured (symbols) microdroplet evaporation rate as a function of contact angle. The effects of changing the contact angle during steady-state water microdroplet evaporation for substrate temperatures ranging between 22℃and 80℃. Data is provided for experiments at three different contact angles.

Figure 4.6 presents evaporation rate as a function of contact angle. Experimentally measured droplet evaporation rates on substrate temperatures are plotted. Multiple steady-state evaporation experiments at droplet contact angles $\{\Theta = 80°, 95°$and $110°\}$ are conducted to understand contact angle relationship to evaporation rate. Substrate temperatures used for the experiments are $22℃ \leq T_{Substrate} \leq 70℃$. A pinned droplet (CCR) is used for all the experiments to avoid contact line influence on evaporation rate. Droplet contact radius for all experiments is R $\cong$ 450 $\pm$ 5 μm. Plot also compares experimental data with numerical simulation results. Experimentally calculated evaporation rates are not dynamic

as in Figure 4.5, but controlled. Numerical predictions by Popov's model [52] and modified Popov's model [56] are used. Along the liquid-vapor interface, Popov's model implement constant surface vapor concentration. Additionally, its predictions fit the evaporation rates at lower substrate temperatures 22℃ $\leq T_{Substrate} \leq$ 50℃. On the contrary, Popov's modified model uses variable surface vapor concentration and its predictions tend to coincide near to saturation temperature, $T_{Substrate} \geq$ 60℃.

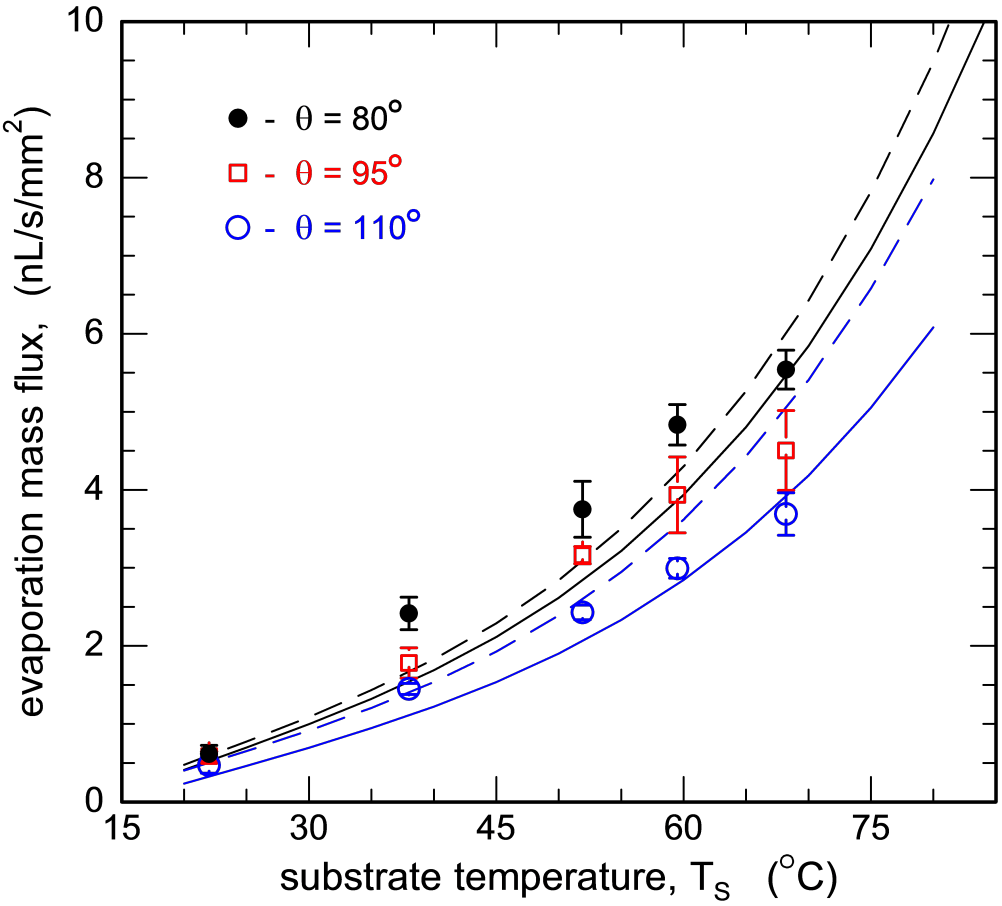

Figure 4.7: Evaporation rate divided by the liquid-vapor surface area plotted as a function of droplet contact angle on substrate temperatures 22℃ $\leq T_{Substrate} \leq$ 70℃. Experimentally measured (symbols) compared to numerical predictions by modified Popovs model with variable surface concentration (solid line) and Popov's model with constant surface concentration (dashed lines).

Figure 4.7 compares evaporation mass flux at contact angles 80°$\leq \Theta \leq$ 110°on substrate temperatures 22℃ $\leq T_{Substrate} \leq$ 70℃. Evaporation rate data from figure 4.6 is divided by

the droplet‘s liquid-vapor surface area for evaporation mass flux. Experimentally calculated evaporation mass fluxes are compared to model predictions. Popov‘s model [52] and Modified Popov‘s model [56] are used for model predictions. As expected, evaporation mass flux decreases with increase in droplet surface area. Figure illustrates a pinned droplet (CCR) at contact angle $\Theta \cong 110^{\circ}$and $80^{\circ}$to have lowest and highest evaporation mass flux respectively. Numerical predictions by modified model at higher temperatures and Popovs model at lower temperatures fit to experimental results. Popov‘s model uses constant vapor concentration over liquid vapor droplet interface causing prediction errors at higher temperatures (temperature distribution varies within the droplet [57, 63, 64]). Temperature gradient within the droplet at lower substrate temperatures $T_{Substrate} \leq 40$℃ is nearly negligible, causing Popov‘s model predictions to coincide with experimental results. The modified model includes variable vapor concentration based on temperature distribution at droplet liquid-vapor interface. Since temperature gradient increases with increase in substrate temperature (droplet apex to substrate temperature vary), incorporated modification to Popov‘s model reduces error and squares experimental results near to saturation temperatures.

Putnam et.al[7] have shown that larger droplets with zero impingement velocity and pinned contact line have increased evaporation rates but reduced heat fluxes. In addition, Garimella et.al‘s [24] vapor diffusion-based model provides reasonable predictions of overall evaporation flux for contact angles ($60^{\circ} \leq \Theta \leq 90^{\circ}$). At these contact angles, evaporative cooling and gas phase convection counterbalance. Evaporative flux predicted by the model at $\Theta = 80^{\circ}$for a 2μL volume droplet at 21℃ coincides with my experimental results.

CHAPTER 5: CONCLUSIONS

Numerous steady state droplet evaporation experiments are conducted at contact angles $80^{\circ} \leq \Theta \leq 110^{\circ}$. A laser patterned moat like trench on the substrate keeps droplet pinned (i.e., constant contact radius mode of evaporation). These experiments are performed at set point temperatures 22℃$\leq \Delta T_0 \leq$ 80℃. Deductions from experimental results and numerical analysis of steady state microdroplet evaporation experiments are reported.

The key conclusions from the experimental study include:

• A microdroplet evaporating at steady state incurs volumetric infuse and evaporation flow rate equilibrium. Droplet parameters {i.e., volume (V), contact radius (R), contact angle (Θ), apex height (H)} remain constant during the evaporation process. Steady state droplet evaporation experiments are conducted to understand contact line and contact angle influence on evaporation rates.

• A water droplet on a heated substrate influences substrate temperature distribution. Energy at higher temperature region (heated substrate) tends to balance lower temperature region (water droplet) through heat transfer, causing substrate cooling. Substrate cooling increases with substrate heating, (i.e.,$T_{Substrate}$ - $T_{Substrate\ cooled}$) increases from $\cong$ 1℃ to $\cong$ 4℃ on substrate temperatures 31℃ $\leq T_{Substrate} \leq$ 68℃. Also, Temperature distribution due to substrate cooling vary radially from the center. Results illustrate lower substrate temperatures near to water droplet than further away. Substrate temperatures at $\sim 800\mu$m and $\sim 2500\mu$m from the center are measured.

• Contact line dynamics on evaporation rate is investigated. Evaporation rate efficiency scales proportional to droplet contact line dynamics. For a pinned droplet (Constant contact radius) evaporation rate remains constant and its efficiency reduces with contact line depinning. Numerical predictions by Popov‘s model and modified Popov‘s model are used for validation of experimental results. Popov model predictions at $T_{Substrate} \leq 40$℃ and modified model predictions at $T_{Substrate} \geq 60$℃ fit to experimental results.

• Experimental investigations reveal contact angle influence on evaporation rate. For a pinned microdroplet (constant contact radius), evaporation rate increases with contact angle ($\dot{m}_{LG} \propto \theta$). Whereas evaporation mass flux decreases with increase in droplet contact angle. Popov‘s model predictions at lower substrate temperatures $T_{Substrate} \leq 40$℃ and modified model predictions near to saturation temperatures $T_{Substrate} \geq 60$℃ validate experimental results.

APPENDIX A: MATLAB CODE TO EVALUATE LOCAL EVAPORATION RATE

```
%This MATLAB code evaluates both Popovs models and the modified
%Popov model with a temperature/cs distribution evaluated using
%the discussed interpolated models.
%
%Written by: Kevin Gleason
%            B.S.A.E - University of Central Florida (2014)
%            M.S.A.E - University of Central Florida (2015)
%
%
%Files need for a working code:
%   Temp_to_Cs_Func.m
%
%
%References:
%
%R. D. Deegan, O. Bakajin, T. F. Dupont, G. Huber, S. R. Nagel,
%   and T. A. Witten. Contact Line Deposits in an Evaporating
%   Drop. Phys. Rev. E, 62:756-765, Jul 2000.
%
%A. M. Briones, J. S. Ervin, L. W. Byrd, S. A. Putnam, A. White,
%   and J. G. Jones. Evaporation Characteristics of Pinned Water
%   Microdroplets. Journal of Thermophysics and Heat Transfer,
%   26:480-493, 2012.
%
%A. Briones, J. Ervin, L. Byrd, S. Putnam, J. Jones, and
%   A. White. Effect of Accommodation Coeffcient, Curvature and
%   Three-Dimensional Flow on the Evaporation Characteristics
%   of Pinned Water Microdroplets. 42nd AIAA Thermophysics
%   Conference, July 2011.
%
%S. Dash and S. V. Garimella. Droplet Evaporation Dynamics on a
%   Superhydrophobic Surface with Negligible Hysteresis.
%   Langmuir, 29(34):10785-10795, 2013.
%
%K. Gleason, and S. A. Putnam. Microdroplet evaporation with a
%   forced pinned contact line. Langmuir, 30(34):10548-10555,
%   2014.
%
%
clear all


```

```
for Ts_input = 20:5:90
%%%%%%%%%%%%%%%%%%%%%%%%%%%%%%%%%%%%%%%%%%%%%%%%%%%%%%%%%%%%%%%%%%%%%%%
%%%%%%%%%%%%%%%%%%%%%%%%%%%%%%%%%%%%%%%%%%%%%%%%%%%%%%%%%%%%%%%%%%%%%%%
% Below are a few options to create the desired plot
%-------------------------------------------------------------------
%% Variable C_s Model
yn_cs = 1;
        %1 - Constant surface concentation (Popov's Model)
        %2 - Temperature distribution (Modified Popov Model)

%-------------------------------------------------------------------
%-------------------------------------------------------------------
%% Experimental Data Input

%Manual Data input (for Local Evap evaluation)
manual_theta_deg = 110; %degrees
manual_radius = 450; %um
% Ts_input = 42; %C

%-------------------------------------------------------------------
% This ends the user input section.  Below is the evaluation
%%%%%%%%%%%%%%%%%%%%%%%%%%%%%%%%%%%%%%%%%%%%%%%%%%%%%%%%%%%%%%%%%%%%%%%
%%%%%%%%%%%%%%%%%%%%%%%%%%%%%%%%%%%%%%%%%%%%%%%%%%%%%%%%%%%%%%%%%%%%%%%


%% Vector Inputs for Variable Surface Concentration
    Ts = Ts_input - ... %Ts Controller
        (-0.00162*Ts_input^2 + 0.40216*Ts_input -9.0647);
    if yn_cs == 1;
        c_s = Temp_to_Cs_Func(Ts);
    elseif yn_cs == 2
            run('Briones_Data')
                alpha_B = alpha; %avoid overwriting alpha
                theta_B = theta; %avoid overwriting theta
            run('Dash_Data')
                alpha = [alpha_B, alpha]; %compiling data sets
                theta = [theta_B, theta]; %compiling data sets
            Temp_Dist = [Normed_Temp_Briones, Normed_Temp_Dash];
            c_s = Temp_to_Cs_Func(Ts*Temp_Dist);
            cs_fit = fit([alpha', theta'], c_s, 'poly22');
    else
            disp('Reason for error:')
```

```
85              disp('Invalid yn_cs Value')
86      end
87
88  %% Data Calling
89  R_dat = manual_radius*10^(-3); %mm
90  theta_dat = manual_theta_deg;
91      theta_rad = manual_theta_deg*pi/180; %convert to radians
92  Vi = ((pi*manual_radius^3) / (3 * sin(theta_rad)^3)) * ...
93      (2 - 3*cos(theta_rad) + (cos(theta_rad))^3) * 10^-6; %nL
94
95  %Other parameters
96  D = 26.1; %mm^2/s
97  c_inf = 0.56*Temp_to_Cs_Func(21); %56% humidity at 21deg
98
99  %%%%%  Integration Parameters  %%%%%
100 %defining 'tau' [t] limits and step size
101 t_del = 1e-2;
102 t_max = 10;
103 t_iter = t_max/t_del;
104
105 %defining 'xi' [x] limits and step size
106 %   (legendre function integration)
107 x_del = 1e-2;
108 x_max = 10;
109 x_iter = x_max/x_del;
110
111 %defining limit and step size of alpha [a]
112 alpha_vec = 10^-3:10^-3:5;
113
114
115 %%  Begin Evaluation  %%%%%
116         theta = theta_dat*pi/180; %converting to radians
117         R = R_dat;
118         alpha = alpha_vec;
119
120      if yn_cs ~= 1;
121          c_s = cs_fit(alpha,theta);
122      else
123          c_s(1:length(alpha_vec)) = c_s;
124      end
125
126 %calculating dM/dt
```

```
    for ii = 1:t_iter
        t1 = (ii-1)*t_del;
        t2 = (ii)*t_del;
            if t1 == 0 %singularity at 1/sinh(0)
                t1 = 10^-4;
            end
        M_int(ii) = t_del/2 * ((((1 + cosh(2*theta*t1)) / ...
            (sinh(2*pi * t1))) * (tanh((pi - theta) * t1))) ...
            + (((1 + cosh(2*theta*t2)) / (sinh(2*pi*t2))) * ...
            (tanh((pi - theta) * t2))));
    end

    M = (-pi * R * D * (c_s - c_inf) * (sin(theta) / ...
        (1 + cos(theta)) + 4 * sum(M_int))) * ...
        (10^6); %converting to ug (result is ug/s OR nL/s)

%Rate of Volume loss
radius_steps = sinh(alpha)./(cosh(alpha)-cos(pi-theta));
    for ij = 1:length(radius_steps)-1
        dR_step(ij) = radius_steps(ij+1) - radius_steps(ij);
        dMass(ij) = M(ij) + M(ij+1);
        LocalInt(ij) = abs(dMass(ij)).*abs(dR_step(ij))/2;
    end

LocalEvapRate = sum(LocalInt);
x = sprintf('Local Evaporation Rate for: Theta = %4.1f', ...
    manual_theta_deg, Ts_input, LocalEvapRate);
disp(x)
end
```

REFERENCES

[1] M. Schena, D. Shalon, R. W. Davis, and P. O. Brown. Quantitative monitoring of gene expression patterns with a complementary DNA microarray. *Science*, 270(5235):467–470, 1995.

[2] V. Dugas, J. Broutin, and E. Souteyrand. Droplet evaporation study applied to DNA chip manufacturing. *Langmuir*, 21(20):9130–9136, 2005.

[3] J. Park and J. Moon. Control of colloidal particle deposit patterns within picoliter droplets ejected by ink-jet printing. *Langmuir*, 22(8):3506–3513, 2006.

[4] G. Li, S. M. Flores, C. Vavilala, M. Schmittel, and K. Graf. Evaporation dynamics of microdroplets on self-assembled monolayers of dialkyl disulfides. *Langmuir*, 25(23):13438–13447, 2009.

[5] W. Deng and A. Gomez. Electrospray cooling for microelectronics. *International Journal of Heat and Mass Transfer*, 54(11):2270–2275, 2011.

[6] A. M. Briones, J. S. Ervin, S. A. Putnam, L. W. Byrd, and L. Gschwender. Micrometer-sized water droplet impingement dynamics and evaporation on a flat dry surface. *Langmuir*, 26(16):13272–13286, 2010.

[7] S. A. Putnam, A. M. Briones, L. W. Byrd, J. S. Ervin, M. S. Hanchak, A. White, and J. G. Jones. Microdroplet evaporation on superheated surfaces. *International Journal of Heat and Mass Transfer*, 55(21):5793–5807, 2012.

[8] S. A. Putnam, L. W. Byrd, A. M. Briones, M. S. Hanchak, J. S. Ervin, and J. G. Jones. Role of entrapped vapor bubbles during microdroplet evaporation. *Applied Physics Letters*, 101(7):071602, 2012.

[9] T. J. Hartranft and G. S. Settles. Sheet atomization of non-Newtonian liquids. *Atomization and Sprays*, 13(2&3), 2003.

[10] S. A. Putnam, A. M. Briones, J. S. Ervin, M. S. Hanchak, L. W. Byrd, and J. G. Jones. Interfacial heat transfer during microdroplet evaporation on a laser heated surface. *International Journal of Heat and Mass Transfer*, 55(23):6307–6320, 2012.

[11] C. D. Whiteman. *Mountain meteorology: fundamentals and applications*. Oxford University Press, 2000.

[12] E. Bormashenko, A. Musin, and M. Zinigrad. Evaporation of droplets on strongly and weakly pinning surfaces and dynamics of the triple line. *Colloids and Surfaces A: Physicochemical and Engineering Aspects*, 385(1):235–240, 2011.

[13] R. Mollaret, K. Sefiane, J. Christy, and D. Veyret. Experimental and numerical investigation of the evaporation into air of a drop on a heated surface. *Chemical Engineering Research and Design*, 82(4):471–480, 2004.

[14] P. G. Pittoni, C.-C. Chang, T.-S. Yu, and S.-Y. Lin. Evaporation of water drops on polymer surfaces: pinning, depinning and dynamics of the triple line. *Colloids and Surfaces A: Physicochemical and Engineering Aspects*, 432:89–98, 2013.

[15] M. A. Saada, S. Chikh, and L. Tadrist. Evaporation of a sessile drop with pinned or receding contact line on a substrate with different thermophysical properties. *International Journal of Heat and Mass Transfer*, 58(1):197–208, 2013.

[16] D. Hu, H. Wu, and Z. Liu. Effect of liquid–vapor interface area on the evaporation rate of small sessile droplets. *International Journal of Thermal Sciences*, 84:300–308, 2014.

[17] P.-G. De Gennes, F. Brochard-Wyart, and D. Quéré. *Capillarity and wetting phenomena: drops, bubbles, pearls, waves*. Springer Science & Business Media, 2013.

[18] R. Wang. KS Birdi: Handbook of Surface and Colloid Chemistry, (CRC Press, Boca Raton, London, New York, Washington, DC, ISBN 0–8493–1079–2, acid-free paper, 765 pages, Price: 182£). *Colloid and Polymer Science*, 282(11):1298–1298, 2004.

[19] J. Zhang, F. Leroy, and F. Müller-Plathe. Influence of Contact-Line Curvature on the Evaporation of Nanodroplets from Solid Substrates. *Physical review letters*, 113(4):046101, 2014.

[20] H. Hu and R. G. Larson. Evaporation of a sessile droplet on a substrate. *The Journal of Physical Chemistry B*, 106(6):1334–1344, 2002.

[21] J. J. Hegseth, N. Rashidnia, and A. Chai. Natural convection in droplet evaporation. *Physical review E*, 54(2):1640, 1996.

[22] P. Kelly-Zion, C. J. Pursell, N. Hasbamrer, B. Cardozo, K. Gaughan, and K. Nickels. Vapor distribution above an evaporating sessile drop. *International Journal of Heat and Mass Transfer*, 65:165–172, 2013.

[23] S. Dehaeck, A. Rednikov, and P. Colinet. Vapor-based interferometric measurement of local evaporation rate and interfacial temperature of evaporating droplets. *Langmuir*, 30(8):2002–2008, 2014.

[24] Z. Pan, J. A. Weibel, and S. V. Garimella. Influence of surface wettability on transport mechanisms governing water droplet evaporation. *Langmuir*, 30(32):9726–9730, 2014.

[25] A. Fujita, R. Kurose, and S. Komori. Experimental study on effect of relative humidity on heat transfer of an evaporating water droplet in air flow. *International Journal of Multiphase Flow*, 36(3):244–247, 2010.

[26] L. Biswal, S. Som, and S. Chakraborty. Thin film evaporation in microchannels with slope-and curvature-dependent disjoining pressure. *International Journal of Heat and Mass Transfer*, 57(1):402–410, 2013.

[27] D. Orejon, K. Sefiane, and M. E. Shanahan. Stick–slip of evaporating droplets: substrate hydrophobicity and nanoparticle concentration. *Langmuir*, 27(21):12834–12843, 2011.

[28] J. R. Moffat, K. Sefiane, and M. E. Shanahan. Effect of TiO2 nanoparticles on contact line stick- slip behavior of volatile drops. *The Journal of Physical Chemistry B*, 113(26):8860–8866, 2009.

[29] R. Craster, O. Matar, and K. Sefiane. Pinning, retraction, and terracing of evaporating droplets containing nanoparticles. *Langmuir*, 25(6):3601–3609, 2009.

[30] H. Bodiguel, F. Doumenc, and B. Guerrier. Stick- slip patterning at low capillary numbers for an evaporating colloidal suspension. *Langmuir*, 26(13):10758–10763, 2010.

[31] R. Picknett and R. Bexon. The evaporation of sessile or pendant drops in still air. *Journal of Colloid and Interface Science*, 61(2):336–350, 1977.

[32] W. Xu, R. Leeladhar, Y. T. Kang, and C.-H. Choi. Evaporation kinetics of sessile water droplets on micropillared superhydrophobic surfaces. *Langmuir*, 29(20):6032–6041, 2013.

[33] M. E. Shanahan. Simple theory of" stick-slip" wetting hysteresis. *Langmuir*, 11(3):1041–1043, 1995.

[34] T. A. Nguyen and A. V. Nguyen. On the lifetime of evaporating sessile droplets. *Langmuir*, 28(3):1924–1930, 2012.

[35] N. Anantharaju, M. Panchagnula, and S. Neti. Evaporating drops on patterned surfaces: Transition from pinned to moving triple line. *Journal of colloid and interface science*, 337(1):176–182, 2009.

[36] S. Chandra, M. Di Marzo, Y. Qiao, and P. Tartarini. Effect of liquid-solid contact angle on droplet evaporation. *Fire Safety Journal*, 27(2):141–158, 1996.

[37] E. F. Crafton and W. Black. Heat transfer and evaporation rates of small liquid droplets on heated horizontal surfaces. *International Journal of Heat and Mass Transfer*, 47(6):1187–1200, 2004.

[38] S. David, K. Sefiane, and L. Tadrist. Experimental investigation of the effect of thermal properties of the substrate in the wetting and evaporation of sessile drops. *Colloids and Surfaces A: Physicochemical and Engineering Aspects*, 298(1):108–114, 2007.

[39] T. A. Nguyen, A. V. Nguyen, M. A. Hampton, Z. P. Xu, L. Huang, and V. Rudolph. Theoretical and experimental analysis of droplet evaporation on solid surfaces. *Chemical Engineering Science*, 69(1):522–529, 2012.

[40] D. H. Shin, S. H. Lee, J.-Y. Jung, and J. Y. Yoo. Evaporating characteristics of sessile droplet on hydrophobic and hydrophilic surfaces. *Microelectronic Engineering*, 86(4):1350–1353, 2009.

[41] V. Starov and K. Sefiane. On evaporation rate and interfacial temperature of volatile sessile drops. *Colloids and Surfaces A: Physicochemical and Engineering Aspects*, 333(1):170–174, 2009.

[42] Y.-S. Yu, Z. Wang, and Y.-P. Zhao. Experimental and theoretical investigations of evaporation of sessile water droplet on hydrophobic surfaces. *Journal of colloid and interface science*, 365(1):254–259, 2012.

[43] A. Oláh and G. J. Vancso. Characterization of adhesion at solid surfaces: Development of an adhesion-testing device. *European polymer journal*, 41(12):2803–2823, 2005.

[44] Z. Pan, S. Dash, J. A. Weibel, and S. V. Garimella. Assessment of water droplet evaporation mechanisms on hydrophobic and superhydrophobic substrates. *Langmuir*, 29(51):15831–15841, 2013.

[45] M. Reyssat and D. Quéré. Contact Angle Hysteresis Generated by Strong Dilute Defects. *The Journal of Physical Chemistry B*, 113(12):3906–3909, 2009.

[46] R. Tadmor, P. Bahadur, A. Leh, H. E. Nguessan, R. Jaini, and L. Dang. Measurement of lateral adhesion forces at the interface between a liquid drop and a substrate. *Physical review letters*, 103(26):266101, 2009.

[47] H. Gelderblom, A. G. Marin, H. Nair, A. van Houselt, L. Lefferts, J. H. Snoeijer, and D. Lohse. How water droplets evaporate on a superhydrophobic substrate. *Physical Review E*, 83(2):026306, 2011.

[48] H. Y. Erbil. Evaporation of pure liquid sessile and spherical suspended drops: A review. *Advances in Colloid and Interface Science*, 170(1):67–86, 2012.

[49] T. A. Nguyen and A. V. Nguyen. Increased evaporation kinetics of sessile droplets by using nanoparticles. *Langmuir*, 28(49):16725–16728, 2012.

[50] H. Song, Y. Lee, S. Jin, H.-Y. Kim, and J. Y. Yoo. Prediction of sessile drop evaporation considering surface wettability. *Microelectronic Engineering*, 88(11):3249–3255, 2011.

[51] Y.-S. Yu, Z. Wang, and Y.-P. Zhao. Experimental and theoretical investigations of evaporation of sessile water droplet on hydrophobic surfaces. *Journal of colloid and interface science*, 365(1):254–259, 2012.

[52] Y. O. Popov. Evaporative deposition patterns: spatial dimensions of the deposit. *Physical Review E*, 71(3):036313, 2005.

[53] R. D. Deegan, O. Bakajin, T. F. Dupont, G. Huber, S. R. Nagel, and T. A. Witten. Contact line deposits in an evaporating drop. *Physical review E*, 62(1):756, 2000.

[54] S. David, K. Sefiane, and L. Tadrist. Experimental investigation of the effect of thermal properties of the substrate in the wetting and evaporation of sessile drops. *Colloids and Surfaces A: Physicochemical and Engineering Aspects*, 298(1):108–114, 2007.

[55] J. M. Stauber, S. K. Wilson, B. R. Duffy, and K. Sefiane. Evaporation of Droplets on Strongly Hydrophobic Substrates. *Langmuir*, 31(12):3653–3660, 2015.

[56] K. Gleason and S. A. Putnam. Microdroplet evaporation with a forced pinned contact line. *Langmuir*, 30(34):10548–10555, 2014.

[57] S. Dash and S. V. Garimella. Droplet evaporation dynamics on a superhydrophobic surface with negligible hysteresis. *Langmuir*, 29(34):10785–10795, 2013.

[58] F. Carle, B. Sobac, and D. Brutin. Experimental evidence of the atmospheric convective transport contribution to sessile droplet evaporation. *Applied Physics Letters*, 102(6):061603, 2013.

[59] A. M. Briones, J. S. Ervin, L. W. Byrd, S. A. Putnam, A. White, and J. G. Jones. Evaporation characteristics of pinned water microdroplets. *Journal of Thermophysics and Heat Transfer*, 26(3):480–493, 2012.

[60] T. A. Nguyen, A. V. Nguyen, M. A. Hampton, Z. P. Xu, L. Huang, and V. Rudolph. Theoretical and experimental analysis of droplet evaporation on solid surfaces. *Chemical Engineering Science*, 69(1):522–529, 2012.

[61] D. H. Shin, S. H. Lee, J.-Y. Jung, and J. Y. Yoo. Evaporating characteristics of sessile droplet on hydrophobic and hydrophilic surfaces. *Microelectronic Engineering*, 86(4):1350–1353, 2009.

[62] K. Birdi, D. Vu, and A. Winter. A study of the evaporation rates of small water drops placed on a solid surface. *The Journal of physical chemistry*, 93(9):3702–3703, 1989.

[63] A. M. Briones, J. S. Ervin, L. W. Byrd, S. A. Putnam, A. White, and J. G. Jones. Effect of accommodation coefficient, curvature and three-dimensional flow on the evaporation characteristics of pinned water microdroplets. 2011.

[64] A. M. Briones, J. S. Ervin, L. W. Byrd, S. A. Putnam, A. White, and J. G. Jones. Evaporation characteristics of pinned water microdroplets. *Journal of Thermophysics and Heat Transfer*, 26(3):480–493, 2012.